Letter

Merging plasmonic and geometric phase in continuously shaped metasurfaces for arbitrary orbital angular momentum

Yinghui Guo, Mingbo Pu, Zeyu Zhao, Yanqin Wang, Jinjin Jin, Ping Gao, Xiong Li, Xiaoliang Ma, and Xiangang Luo

ACS Photonics, **Just Accepted Manuscript** • DOI: 10.1021/acsphotonics.6b00564 • Publication Date (Web): 13 Oct 2016

Merging geometric phase and plasmon retardation phase in continuously shaped metasurfaces for arbitrary orbital angular momentum generation

Yinghui Guo‡, Mingbo Pu‡, Zeyu Zhao‡, Yanqin Wang, JinJin Jin, Ping Gao, Xiong Li, Xiaoliang Ma, and Xiangang Luo*

State Key Laboratory of Optical Technologies on Nano-Fabrication and Micro-Engineering, Institute of Optics and Electronics, Chinese Academy of Sciences, P.O. Box 350, Chengdu 610209, China

‡*Y. Guo, M. Pu, Z. Zhao contributed equally to this work*

E-mail: lxg@ioe.ac.cn

Abstract

Traditional technologies to generate and manipulate the orbital angular momentum (OAM) surfer from bulky size and do not lend themselves to nanophotonic system. Ultrathin metasurface based on abrupt phase shift has recently been proposed as an alternative method. Nevertheless, gradient phase was generally approximated by multiple meta-atom/molecules with discrete levels of abrupt phase shift, which not only increase the design and fabrication complexity but also cause difficulties in obtaining simultaneous electrical and optical functionality. Furthermore, discontinuous phase profile would introduce phase noise to the scattering fields and deteriorate the purity of the OAM beams. Here, we propose a wave-front engineering mechanism by virtue of the spin-orbit interaction (SOI) in continuously shaped plasmonic metasurfaces, which offers a new approach to generate OAM modes of high purity. Equally important, a method producing arbitrary OAM topological,

integer and fractional, is demonstrated by merging plasmon retardation phase with geometric phase in the proposed continuously shaped metasurfaces. The proposed approach is well supported by full-wave numerical simulations and experimental characterization of the fabricated structure in the visible regime.

Keywords:

metasurface, orbital angular momentum, spin-orbit interaction, plasmon retardation phase

A critical issue in optical communications is that the exponential growth of data traffic will exhaust the available capacity in the near future. Over the past 40 years, a set of technological breakthroughs has emerged to address the forecasted upcoming "capacity crunch".[1] In conjunction with digital coherent receivers, advance modulation formats and time/wavelength/polarization multiplexing technologies are pushing transmission efficiency close to the Shannon's limit.[2] Avoiding the Shannon limit requires taking the remaining untapped spatial dimension.[1] Recent progresses in modal basis sets that carry orbital angular momentum (OAM) facilitate space-division multiplexing due to the inherent orthogonality of the different OAM modes.[3,4]

Angular momentum encompasses spin angular momentum (SAM) and OAM. Spin photon carrying $\sigma\hbar$ of angular momentum is manifested as circular polarization, where $\hbar$ is the reduced Plank's constant, $\sigma = \pm 1$ corresponds to the left circularly polarized (LCP) and right circularly polarized (RCP) light, respectively. OAM is related to the spatial distribution, i.e., the optical phase profile of the beam. It was shown by Allen in 1992 that light beams having an azimuthal phase $\exp(i\ell\phi)$ carried

an OAM of $\ell\hbar$ per photon, where, ϕ is the azimuthal coordinate, ℓ is referred to as the topological charge of the beam.[5,6] Dissimilar to the SAM, OAM theoretically has unbounded quantum states and thus has the potential to tremendously increase the capacity of communication systems. Because of the unique energy distribution, OAM-carrying beams also play vital role in optical microscopy, optical manipulation,[7] and physics detection. OAM carrying beams have been successfully generated by space light modulator, spiral phase plates, *q*-plates (inhomogeneous birefringent media), and astigmatic mode converters.[8,9] However, the employed devices are cumbersome and cannot meet the trend of integration.

Surface plasmon polaritons (SPPs) have created an appealing platform for designing various optical components with small footprints.[10–12] The initial proposals of optical beaming, focusing and subwavelength imaging in variant width metallic apertures/slits indicate that the plasmon retardation effect can be taken as pioneering planning of phase discontinuity metasurface.[13] The local phase abrupt induced by plasmon retardation effect of metallic slits also find applications in OAM generation[14] and two dimensional lensing.[15] Recently, phase-change material is introduced into the metallic slits to realize tunable nanophotonic components.[16,17] Phase discontinuity is subsequently fostered in elaborately designed plasmonic resonant modes,[18–20] arranging in two-dimensional metal-dielectric interface, also recognized as metasurfaces. Owing to the abrupt phase change, traditional law of reflection should be revised accordingly and replaced by the metasurface-assisted law of refraction and reflection (MLRR).[13] Moreover, the traditional Fresnel's equations can also be revised

via the metasurface/metamirror approach.[21,22] In order to circumvent the disadvantages of narrow operation bandwidths and high losses in original resonant metasurface, geometric phase stemming from the spin-orbit interaction (SOI) in inhomogeneous and anisotropic structures is taken as one promising alternative for gradient metasurface. Benefiting from the frequency independent properties, geometric metasurfaces have been employed in numerous broadband optical devices.[23–28]

It is worth to note that, most previous gradient metasurfaces are constructed by a serial of discrete meta-atoms. Gradient phase was approximated by discrete levels of abrupt phase shift. On one hand, it is a significant challenge obtaining high-performance metasurfaces that can operate at visible frequency range with high uniformity.[29] On the other hand, the discontinuous nature inevitably degrades the overall performance of metasurfaces, for example, decreasing the purity of generated OAM and causing aberrations in imaging and focusing system. Besides, discrete system is not electrically conductive, thus it is difficult to obtain simultaneous electric and optical functionality. Quite recently, quasi-continuous super-meta-atoms including catenary and trapezoid shaped structure are adopted in metasurfaces to overcome the shortages above.[30–33]

In this paper, we present a metasurface constructed by true continuous super-meta-atoms i.e., plasmonic annular apertures, as shown in Figure 1a. On one hand, the spatial inhomogeneity and strong anisotropy of the annular apertures arouse the SOI in the proposed metasurface and generate continuous geometric phase shift.

On the other hand, by smoothly changing the width of the annular apertures, another continuous phase shift, plasmon retardation phase, can be obtained. By merging of two continuous phase shift above in single metasurface, we can realize arbitrary (integer and fractional) OAM generation. The proposed approach is well validated by both the vectorial angular spectrum theory (VAST)[34,35] and the experiments in visible band. The suggested method opens an avenue to generate continuous gradient phase using a single metasurface, offering potential to develop novel compact devices that may lead to advances in a wide range of fields in optics and photonic.

Principle and structure design

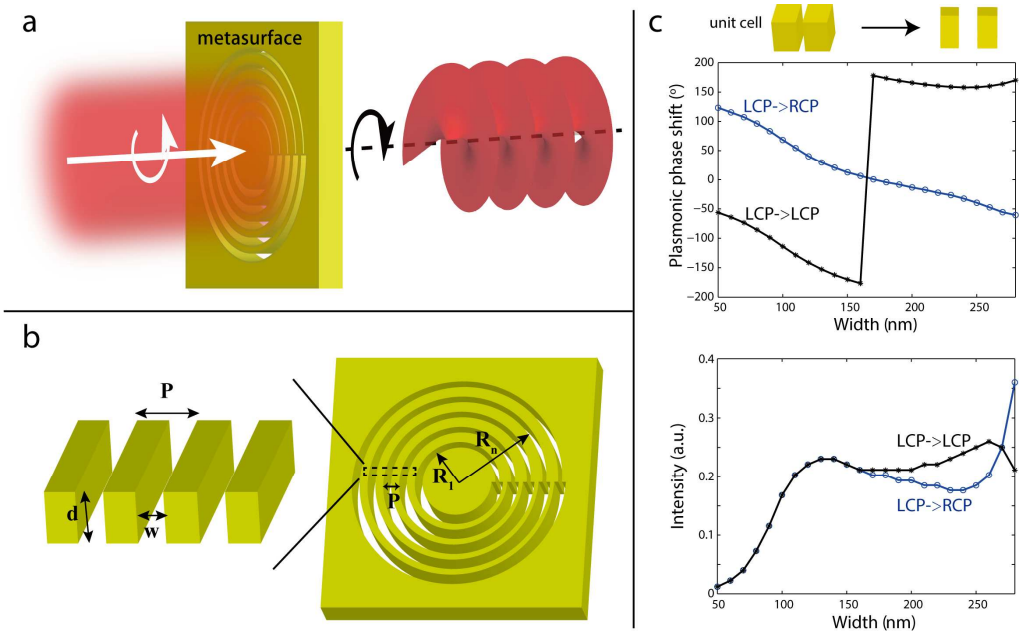

Figure 1. Phase shift mechanism of the proposed metasurface. (a) When a circularly polarized light is normally illuminated on the proposed inhomogeneous and anisotropic metasurface, the transmitted light with opposite handedness possesses a specific phase profile. (b) The metasurface is constructed by drilling a silver film with multiple periods of annular rings, whose radius is defined as $R_n = R_1 + (n\text{-}1)*P$, where n and P delegate the number and the period of the apertures. The annular apertures can be taken regards as two dimensional extension of a set of nanoslits with spatial-varying orientation. (c) The propagation phase shift and intensity of SPP modes as a function of slits width for polarization conversed and conserved terms.

The proposed metasurface is created by drilling an optically thick silver film with annular rings that fully perforating the metallic film. The radius of annular rings are defined as $R_n = R_1 + (n\text{-}1)*P$, where n and P delegate the number and the period of the apertures, as illustrated in Figure 1b. Obviously, our proposed meta-atoms are continuous, which is help to avoid the unanticipated phase noise in discretely shaped metasurface and release the fabrication requirement in visible band. Although similar design has been employed previously in dielectric gratings to generate helical beams, their micron-size features prevent them from working in the visible regime.[36]

Because of the subwavelength aperture width, the proposed metasurface can be taken as a radial polarizer, which only allow the radially polarized components of incidence that orthogonal to the concentric apertures (transverse magnetic polarization with respect to the structure) are coupled to SPP modes and propagate through the apertures. The propagating phase retardation of SPP mode in single metallic slit can be expressed by $\Phi_p = \beta d$, where β and d represent the propagation constant and the depth of the metallic slit, respectively. It is well known that there exists an analytical closed-form for the propagation constant of fundamental SPP mode in isolate subwavelength metallic slit,[37]

$$\tanh(\sqrt{\beta^2 - k_0^2\varepsilon_d}\,\frac{w}{2}) = \frac{-\varepsilon_d\sqrt{\beta^2 - k_0^2\varepsilon_m}}{\varepsilon_m\sqrt{\beta^2 - k_0^2\varepsilon_d}} \quad (1)$$

where, k_0 is the wave vector of light in free space, ε_d and ε_m are the relative dielectric constant for the metal and the materials between slits, and w is the slit width. Through Equation (1) we can obtain the relationship between plasmon phase retardation of with the slit width (see Supplementary Figure S1a).

The proposed metasurface can be taken as a serial of serial of periodic metallic slits with space-variant orientation angle, whose unit cell is shown in Figure 1c. The main difference with discrete meta-atoms array is that the wave-front engineering accuracy is significantly improved because of their nearly infinite small "pixel" size. Subsequently, transmission properties of the unit cell are simulated by using software CST Microwave Studios with periodic boundary condition. The period (P) and depth (d) of the metallic slit are fixed as 400 nm and 450 nm, smaller than the incident wavelength of 632.8 nm, while the slit width (w) changes from 50 nm to 300 nm. It should be noted that, although the theoretical results are consistent with the simulated results of isolate metallic slit, it fails for periodic slits. The simulation results shown in Figure S1b indicate that due to the mutual coupling between neighboring slits, the propagation constant of SPP mode in periodic slits is more sensitive to the slit width variation and thus a larger phase abrupt is obtained between w = 50 nm and w = 300 nm. By filling high refractive index materials in the apertures, the plasmon phase abrupt induced by slit width modulation can expand to 2π.[14]

When the proposed metasurface is normally illuminated by a circularly polarized light (CPL), the output radially polarized components can be decomposed into polarization conversed term and polarization conserved term, whose transmission properties are shown in Figure 1c. One can find that both terms acquire slit width dependent plasmon phase retardation. Because of the handedness insensitive phase retardation, the phase retardation differences between them maintain around π for different slit widths. Besides, when the slit width is smaller than 150 nm, their

intensities are equal and thus the radiated beam can be taken as a radially polarized light (RPL).

For the polarization conversed term, extra geometric phase can be obtain from the spin-orbit interaction (SOI), which can be understood from simple Jones matrix calculations. Mathematically, the relation between the CPL and the RPL can be expressed as:[38]

$$\begin{pmatrix} \overrightarrow{E_r} \\ \overrightarrow{E_\varphi} \end{pmatrix} = \begin{pmatrix} \exp(-j\varphi) & \exp(j\varphi) \\ -j\exp(-j\varphi) & j\exp(j\varphi) \end{pmatrix} \begin{pmatrix} \vec{E}_{LCP} \\ \vec{E}_{RCP} \end{pmatrix} \quad (2)$$

where $\vec{E}_r$, $\vec{E}_\varphi$, $\vec{E}_{LCP}$ and $\vec{E}_{RCP}$ are the electrical field of RPL, azimuthally polarized light (APL), LCP and RCP, respectively. Equation 2 indicates that the output RPL acquires a geometric phase of $\Phi_g = \sigma\varphi$, while the polarization conversed term acquires a geometric phase of $\Phi_g = 2\sigma\varphi$ due to the SOI effect in anisotropic and inhomogeneous media.[30] For the proposed annular apertures, the spatial orientation angle φ changes 2π in a round. Therefore, the radiated RPL would acquire an azimuthal phase shift of $\pm 2\pi$, corresponding to charge of ± 1, while the polarization conversed term acquire an azimuthal phase shift of $\pm 4\pi$, corresponding to charge of ± 2.

The total azimuthal phase shift through the proposed metasurface is the summation of the geometric phase shift and retardation phase shift, which can be expressed by $\Phi = \Phi_g + \Phi_p$. Consequently, we can also obtain arbitrary azimuthal phase shift Φ_p by smoothly changing the width of the annular apertures. For example, if the aperture width anticlockwise increase from 70 nm to 280 nm in a round, the polarization conversed term acquire not only a geometric phase shift of $\Phi_g = \pm 4\pi$ but

also a plasmon retardation phase abrupt of $\Phi_p = -\pi$. The total phase shift Φ is 3π (i.e., ℓ = 1.5 for the case of LCP->RCP) or -5π (i.e., ℓ = -2.5 for the case of RCP->LCP). On the contrary, if the aperture width anticlockwise decrease from 280 nm to 70 nm in a round, Φ_p will be π. The total phase shift Φ is 5π (i.e., ℓ = 2.5 for the case of LCP->RCP) or -3π (i.e., ℓ = -1.5for the case of RCP->LCP). It should be noted that, when we invert the handedness of incidence the topological charge will not only change the sign but also the absolute value.

Results and discussion

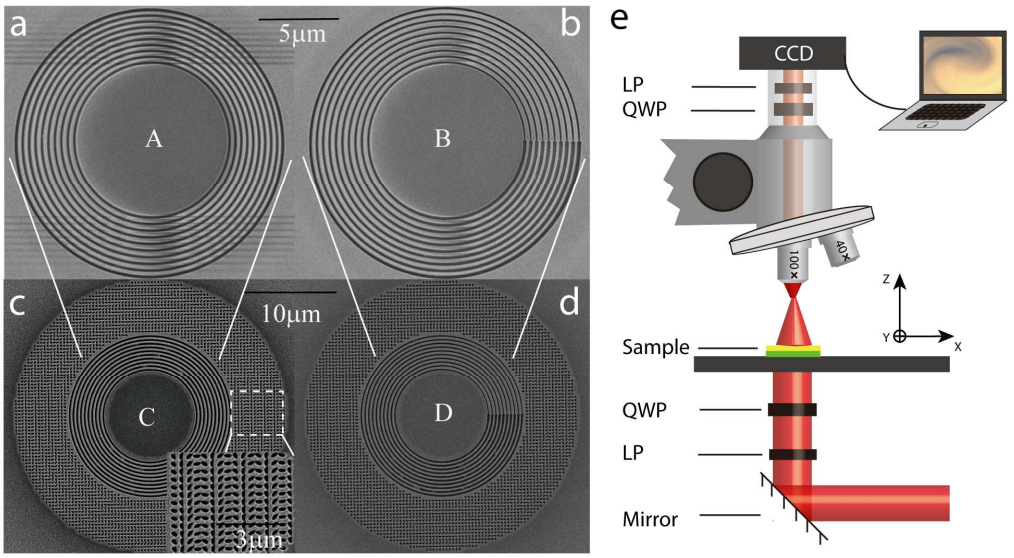

Figure 2. Scanning electron microscopy (SEM) images of fabricated samples and experimental setup. (a) Sample A consists of 10 annular apertures with invariant aperture width w = 200 nm. (b) Sample B consists of 10 annular apertures with w increases anti-clockwise from 70 nm to 280 nm for each ring. (c)(d) Sample C and Sample D include not only the inner annular apertures to produce vortex beams but also outer square lattice of elliptical nanoholes to produce focusing spherical waves. (e) Schematic of the experimental setup. LP: linear polarizer; QWP: quarter-wave plate; CCD: charge-coupled device.

The proposal is firstly investigated by VAST to determine appropriate number and radius of concentric apertures for visible OAM generation. Considering the

meso-field (within several tens of wavelengths from the structure surface) diffraction characteristics of the radiated light as well as the dimensional size of the metasurface (see Supplementary Figure S2 and Figure S3), n and R is selected as 10 and 5 μm respectively in this paper.

Four samples (A, B, C and D) were fabricated by focused ion beam lithography and the scanning electron microscopy (SEM) images are revealed in Figures 2a-2d. Sample A with invariant aperture width w = 200 nm, was designed for the integer OAM generation. Sample B with aperture width w anti-clockwise increases from 70 nm to 280 nm, was designed for the fractional OAM generation. Sample C and Sample D include not only the inner annular apertures to produce vortex beams, but also outer square lattice of elliptical nanoholes with specific orientation (see Supplementary Figure S4) to produce focusing spherical waves. The interference pattern between them at appropriate transverse plane can be utilized to characterize the actual topological charge of generated OAM beams. The schematic of the experimental setup is shown in Figure 2e. The LCP at 632.8 nm is generated by passing a laser beam (HeNe laser) through a properly oriented liner polarizer (LP) and quarter-wave plate (QWP), and then normally illuminated upon the metasurface. Subsequently, the transmitted light passes through a 100× objective, whose focal plane just locates on the output surface of the sample.

In order to examine the polarization of radiated light from sample A, a rotating LP is inserted in our home-built microscope, whose orientation angle is denoted as a white arrow in Figure 3. Note that, the QWP after the objective in Figure 2e is not

inserted in the microscope in this case. The output light is collected by a charge-coupled device (CCD, 1600×1200 pixels, WinCamD-UCD15, DataRayInc) camera. From the results shown in Fig. 3, one can find that the transmitted intensity profiles always exhibit two-lobe shapes and rotate with the LP, signifying the radial polarization of radiated light. In addition, we can clearly observe a typical "s"-shape pattern at the center of the images rotating with the linear polarizer, a direct consequence of the helical phase of the vortex beam with a topological charge of ℓ =1.

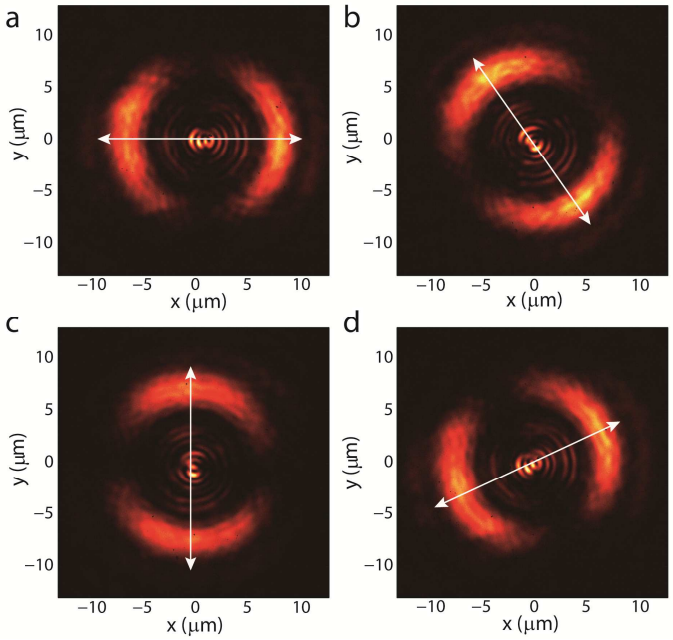

Figure 3. Optical characterization of the radially polarized light generated by Sample A. (a)-(d) Measured transverse intensity profiles after passing a rotating linear polarizer, whose orientation angles is indicated by the white arrows.

Subsequently, we mainly focus on the polarization conversed components that acquiring a geometric phase modulation of $2\sigma\varphi$. To this end, cascaded QWP and LP are utilized and inserted in the microscope to eliminate the co-handed circular polarization component. By recording the transverse snapshots at different distances with an increment of 0.5 μm, we can map out the longitudinal (x-z) intensity

distribution on the transmission side of the Sample A. From Figure 4a, we can see a symmetric hollow beam propagate stably from z = 0 to z = 20 μm, beyond which a continual decay of photon density and gradually decreased confinement of transverse intensity profile are observed. The transverse intensity profile at z = 7 μm, presented in Figure 4b, exhibits a doughnut shape around a dark spot, expected for an integer OAM mode. In contrast, the intensity distribution diffracted by Sample B at the same transverse plane imparts an unclosed C-shape, as illustrated in Figure 4c. Note that, the nonuniform intensity distribution around the singularity in Fig. 4(c) results from the variant slit width, which does not affect the OAM loading.[14] The pseudo-color field maps obtained from VAST are plotted in Figures 4d-4f for comparison. To make the comparisons between the experimental data and theory calculations more clear, we saturate the intensity so the central patterns stand out. Good agreement between them is found considering the fabrication and measurement imperfection. It should be mentioned that the discrepancy for on-axis pattern after 20 μm in Figure 4a may is due to the inclined illumination with respect to the normal direction and residual polarization conserved term (see Supplementary Figure S5a and Figure S5c), which occurs in all probability during the experiments and also cause the central intensity pattern in Figure 4b is spiral-like rather than being concentric rings (see Supplementary Figure S5b and Figure S5d).

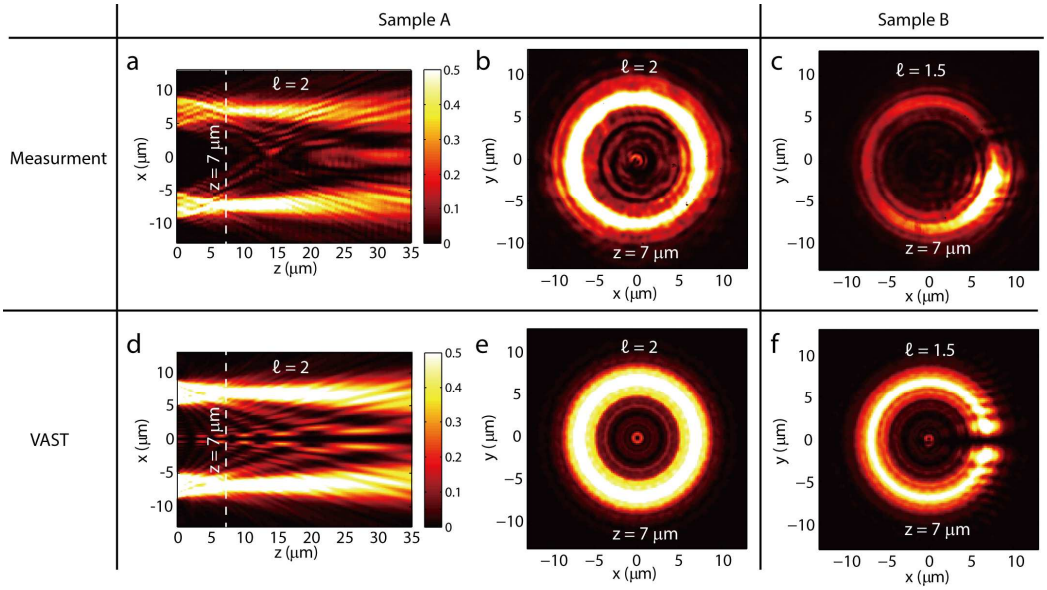

Figure 4. Optical characterization of the diffraction pattern generated by Sample A and Sample B. (a) Measured longitudinal intensity distribution of polarization conversed term on the transmission side of the Sample A. (b) Measured transverse intensity profile at z = 7 μm in (a). (c) Measured transverse intensity profile of Sample B at z = 7 μm. (d)-(f) Corresponding vectorial angular spectrum theory (VAST) results with uniform transmission and ideal phase distribution.

For a complete test, the wave-front shape of polarization conversed components should also be measured to determine the concrete value of the topological charge. In this paper, the interference characterization is performed by the transmission measurement of the Samples C and D, respectively. Compared with previous interferometry,[14,39] additional optical components such as, splitter, coupler and lens are no needed again. Therefore the proposed characterization statics may be more feasible for nanophotonic OAM generators. As indicated in Figure 5a, a focusing spherical wave was generated by the elliptical hole array with the focus spot locating at the position z = 23 μm. Interference pattern generated by Sample C at the transverse plane z = 7 μm is displayed in Figure 5b, which reveals a dual-helix, confirming that the beam carries an OAM value of 2. Interference patterns of Sample D in Figure 5c

demonstrate the generation of fractional OAM value of 1.5. The theoretical calculated results based on VAST are shown in Figures 5d-5f, which elegantly matches well with the experimental measurement results. The small discrepancy between them is owing to the fabrication and measurement imperfections.

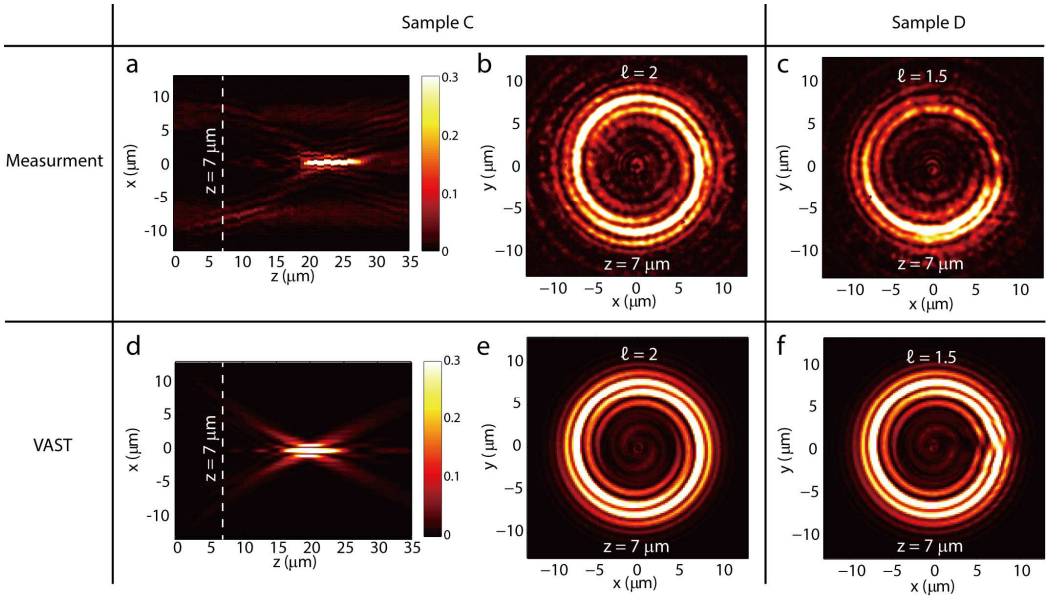

Figure 5. Optical characterization of the diffraction pattern generated by Sample C and D**.** (a) Measured longitudinal intensity distribution of polarization conversed term on the transmission side of the Sample C. (b) Measured transverse intensity profile at z = 7 μm in (a). (c) Measured transverse intensity profile of Sample D at z = 7 μm. (d)-(f) Corresponding VAST results with uniform transmission and ideal phase distribution.

Subsequently, the purity of optical vortex generated from continuously and discretely shaped metasurfaces are compared. To this end, another four samples (E, F, G and H) were fabricated by focused ion beam lithography and the SEM images are revealed in Figures 6a-6d. Sample E (continuously shaped metasurfaces) and Sample F (discretely shaped metasurfaces) have the same inner radius (5 μm), ring number (10), thickness (450 nm), period (400 nm), slit width (150 nm) and the unit cells of them exhibit approximate polarization conversion efficiency (i.e. ~22%, see

Supplementary Figure S6). Sample G(H) includes not only the structures in Sample E(F), but also outer square lattice of elliptical nanoholes with specific orientation, for generation of interference patterns between vortex beam and focusing sphere wave.

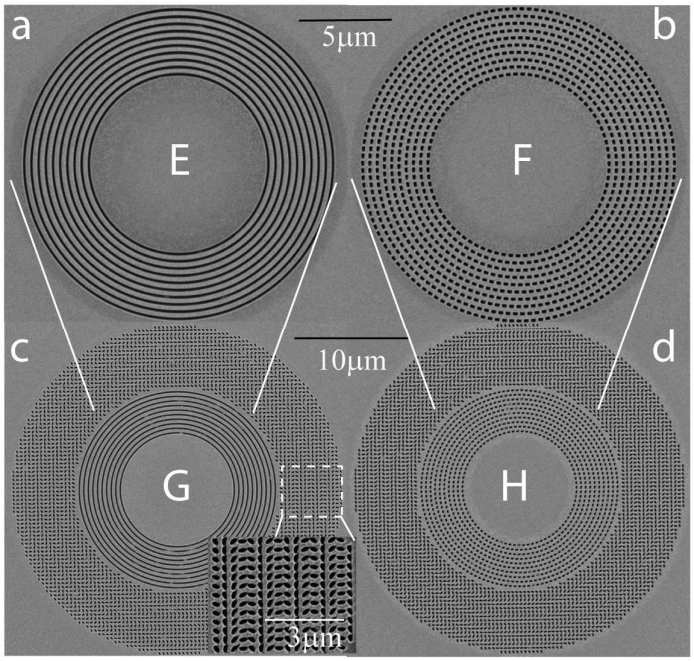

Figure 6. Scanning electron microscopy (SEM) images of fabricated samples**.** (a) SEM of continuously shaped metasurface (Sample E). (b) SEM of discretely shaped metasurface (Sample F). (c) SEM of discretely shaped metasurface. (d) Purity of OAM modes generated by continuously shaped metasurface. (c)(d) Sample G and Sample H include not only the structures in Sample E and Sample F but also outer square lattice of elliptical nanoholes.

Generally, the purity of the optical vortex is calculated by decomposing its complex field on a complete basis set of optical modes with angular momentum, i.e. the Laguerre-Gaussian modes ($E_{l,p}^{LG}$). The weight of a particular LG mode in the vortex beam is calculated by the scalar product: $C_{l,p}^{LG} = \iint_{\infty} E_{vortex} \overline{E_{l,p}^{LG}} dxdy$, where E_{vortex} is the normalized electric field of the generated beam, the integer $p(l)$ is the radial (azimuthal) Laguerre-Gaussian mode index, and the upper bar denotes the complex conjugate[40]. The relative charge distribution of an optical vortex is obtained by

summing all the modes with the same azimuthal index l_0, $C_{l_0} = \sum_p C^{LG}_{p,l_o}$. Since it is difficult to obtain the phase profile by optical measurement, the purity of optical vortex mostly is estimated from the simulation results in previous literatures.[40]

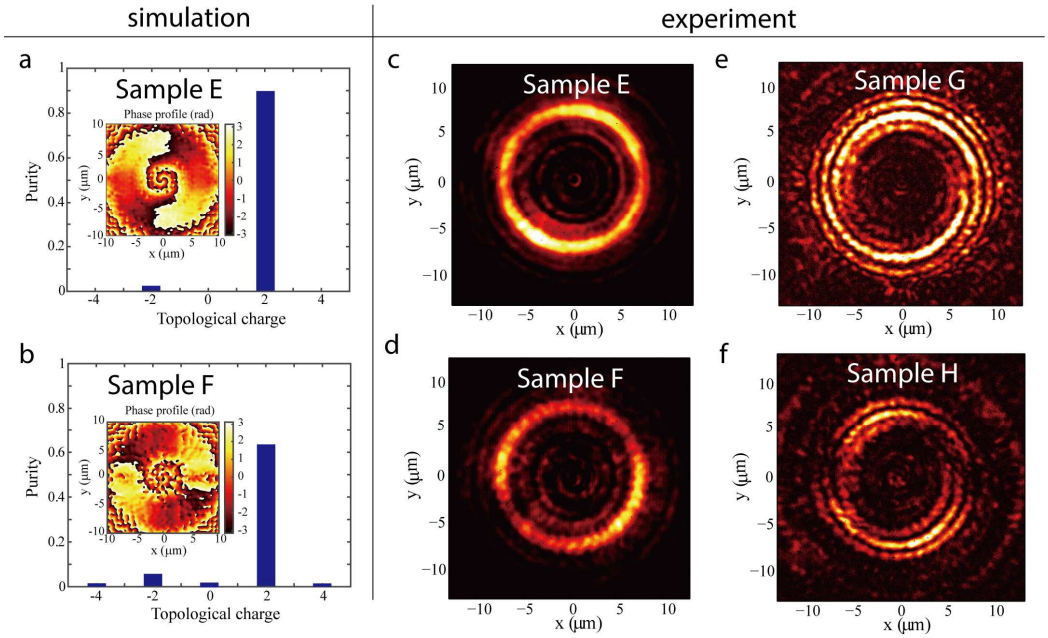

Figure 7. Comparisons between continuously and discretely shaped metasurfaces**.** (a)(b) Purity of OAM modes generated by continuously and discretely shaped metasurface, i.e. sample E and sample F. The insets are the phase profiles at z = 7 shown in the insets. (c)(d) Measured intensity profile from c sample E and sample F. (e)(f) Measured interference pattern from sample G and sample H.

Two histograms representing the relative charge distribution for continuously and discretely shaped metasurfaces are respectively plotted in Figure 7a and Figure 7b, with the corresponding phase profiles at z = 7 shown in the insets. Obviously, the phase noise via continuously shaped metasurface is lower and thus the purity of the single charged vortex (l = 2) created with our technique is above 90%, higher than that of discretely shaped metasurface (~64%). Obviously, the intensity profiles of vortex beams and the interference patterns with focusing wave-front generated by continuously shaped metasurface (Figure 7c and Figure 7e) present higher quality

than those from discretely shaped metasurface (Figure 7e and Figure 7f), which may also stem from the lower phase noise of continuously shaped metasurface. The measured power of polarization conversed and conserved term for sample E are 60 μW and 48 μW, respectively, which means the co-handed CPL wastes about 44% power of the radiated light. In order to improve the overall efficiency, one can use reflective structure to enhance the polarization conversion efficiency (PCE)[41] or replace metal metasurface by low-loss dielectric metasurfaces.[42]

Conclusions

In summary, two different phase modulation scheme, the geometric phase shift and plasmon-induced phase shift, have been combined within single plasmonic metasurface for the generation of both integer and fractional OAM beams. Owing to the continuous phase modulation, phase noises are greatly decreased and much higher purity could be expected. Although only limited topological charges of ±1, ±1.5, ±2, and ±2.5 are discussed in this paper, it is no doubt that other vorticities can also be obtained within the closed-path nanoslits. For example, Brasselet *et al*. has realized the topological shaping of light with different integer OAM by replacing circular metallic nanoslits with multiple circular arc segments.[33,43] By resorting to the methodology above, diversified fractional OAM will be realized and play significant role in the OAM assisted dense mode-division multiplexing (DMDM) systems[44], counterparts of well-known dense wavelength-division multiplexing (DWDM). In addition, merging geometric phase and SPP-inspired phase can be explored for

generation of focusing and high-order Bessel beams possessing OAM by making the aperture width of each slit not same again.

Methods

Microfabrication of Sample: The fabrication began with depositing a 2-nm-thin film of Cr onto a clean and planar quartz substrate to improve the adhesion between the silver film and the substrate. Then a 450-nm-thin silver film was deposited on the quartz substrate by magnetron sputtering in a sputter chamber. Subsequently, annular apertures are created in the silver film using a Ga^+ focused ion beam lithography (FIB, FEI Helios Nanolab 650), and the accelerating voltage and current of the Ga^+ beam were set as 30 kV and 80 pA, respectively.

Acknowledgements

We acknowledge the financial support by 973 Program of China under contract No. 2013CBA01700 and the National Natural Science Foundation of China under grants 61138002 and 61575201.

References

(1) Richardson, D. J.; Fini, J. M.; Nelson, L. E. Space-Division Multiplexing in Optical Fibres. *Nat Photon* **2013**, *7*, 354–362.

(2) R. J. Essiambre; R. W. Tkach. Capacity Trends and Limits of Optical Communication Networks. *Proc. IEEE* **2012**, *100*, 1035–1055.

(3) Gibson, G.; Courtial, J.; Padgett, M. J.; Vasnetsov, M.; Pas'ko, V.; Barnett, S. M.; Franke-Arnold, S. Free-Space Information Transfer Using Light Beams Carrying Orbital Angular Momentum. *Opt. Express* **2004**, *12*, 5448–5456.

(4) Wang, J.; Yang, J.-Y.; Fazal, I. M.; Ahmed, N.; Yan, Y.; Huang, H.; Ren, Y.; Yue, Y.; Dolinar, S.; Tur, M.; Willner, A. E. Terabit Free-Space Data Transmission Employing Orbital Angular Momentum Multiplexing. *Nat. Photonics* **2012**, *6*, 488–496.

(5) Allen, L.; Beijersbergen, M. W.; Spreeuw, R. J. C.; Woerdman, J. P. Orbital Angular-Momentum of Light and the Transformation of Laguerre-Gaussian Laser Modes. *Phys. Rev. A* **1992**, *45*, 8185–8189.

(6) Yao, A. M.; Padgett, M. J. Orbital Angular Momentum: Origins, Behavior and Applications. *Adv. Opt. Photonics* **2011**, *3*, 161–204.

(7) Juan, M. L.; Righini, M.; Quidant, R. Plasmon Nano-Optical Tweezers. *Nat Photon* **2011**, *5*, 349–356.

(8) Heckenberg, N. R.; McDuff, R.; Smith, C. P.; White, A. G. Generation of Optical Phase Singularities by Computer-Generated Holograms. *Opt. Lett.* **1992**, *17*, 221–223.

(9) Marrucci, L.; Manzo, C.; Paparo, D. Optical Spin-to-Orbital Angular Momentum Conversion in Inhomogeneous Anisotropic Media. *Phys. Rev. Lett.* **2006**, *96*, 163905.

(10) Atwater, H. A. The Promise of Plasmonics. *Sci. Am.* **2007**, *296*, 56–62.

(11) Polman, A.; Atwater, H. A. Plasmonics: Optics at the Nanoscale. *Mater. Today* **2005**, *8*, 56.

(12) Maier, S. A. *Plasmonics: Fundamentals and Applications*; Springer: New York, 2007.

(13) Luo, X. Principles of Electromagnetic Waves in Metasurfaces. *Sci. China-Phys. Mech. Astron.* **2015**, *58*, 594201.

(14) Sun, J.; Wang, X.; Xu, T.; Kudyshev, Z. A.; Cartwright, A. N.; Litchinitser, N. M. Spinning Light on the Nanoscale. *Nano Lett.* **2014**, *14*, 2726–2729.

(15) Ishii, S.; Shalaev, V. M.; Kildishev, A. V. Holey-Metal Lenses: Sieving Single Modes with Proper Phases. *Nano Lett.* **2013**, *13*, 159−163.

(16) Chen, Y.; Li, X.; Sonnefraud, Y.; Fernández-Domínguez, A. I.; Luo, X.; Hong, M.; Maier, S. A. Engineering the Phase Front of Light with Phase-Change Material Based Planar Lenses. *Sci. Rep.* **2015**, *5*, 8660.

(17) Rudé, M.; Simpson, R. E.; Quidant, R.; Pruneri, V.; Renger, J. Active Control of Surface Plasmon Waveguides with a Phase Change Material. *ACS Photonics* **2015**, *2*, 669–674.

(18) Yu, N.; Genevet, P.; Kats, M. A.; Aieta, F.; Tetienne, J.-P.; Capasso, F.; Gaburro, Z. Light Propagation with Phase Discontinuities: Generalized Laws of Reflection and Refraction. *Science* **2011**, *334*, 333–337.

(19) Zhang, X.; Tian, Z.; Yue, W.; Gu, J.; Zhang, S.; Han, J.; Zhang, W. Broadband Terahertz Wave Deflection Based on C-Shape Complex Metamaterials with Phase Discontinuities. *Adv. Mater.* **2013**, *25*, 4567–4572.

(20) Sun, S.; Yang, K. Y.; Wang, C. M.; Juan, T. K.; Chen, W. T.; Liao, C. Y.; He, Q.; Xiao, S.;

Kung, W. T.; Guo, G. Y.; Zhou, L.; Tsai, D. P. High-Efficiency Broadband Anomalous Reflection by Gradient Meta-Surfaces. *Nano Lett.* **2012**, *12*, 6223−6229.

(21) Esfandyarpour, M.; Garnett, E. C.; Cui, Y.; McGehee, M. D.; Brongersma, M. L. Metamaterial Mirrors in Optoelectronic Devices. *Nat. Nanotechnol.* **2014**, *9*, 542.

(22) Guo, Y.; Wang, Y.; Pu, M.; Zhao, Z.; Wu, X.; Ma, X.; Wang, C.; Yan, L.; Luo, X. Dispersion Management of Anisotropic Metamirror for Super-Octave Bandwidth Polarization Conversion. *Sci. Rep.* **2015**, *5*, 8434.

(23) Chen, X.; Huang, L.; Mühlenbernd, H.; Li, G.; Bai, B.; Tan, Q.; Jin, G.; Qiu, C. W.; Zhang, S.; Zentgraf, T. Dual-Polarity Plasmonic Metalens for Visible Light. *Nat. Commun.* **2012**, *3*, 1198.

(24) Du, L.; Kou, S. S.; Balaur, E.; Cadusch, J. J.; Roberts, A.; Abbey, B.; Yuan, X.-C.; Tang, D.; Lin, J. Broadband Chirality-Coded Meta-Aperture for Photon-Spin Resolving. *Nat Commun* **2015**, *6*.

(25) Huang, L.; Chen, X.; Mühlenbernd, H.; Li, G.; Bai, B.; Tan, Q.; Jin, G.; Zentgraf, T.; Zhang, S. Dispersionless Phase Discontinuities for Controlling Light Propagation. *Nano Lett.* **2012**, *12*, 5750–5755.

(26) Ni, X.; Wong, Z. J.; Mrejen, M.; Wang, Y.; Zhang, X. An Ultrathin Invisibility Skin Cloak for Visible Light. *Science* **2015**, *349*, 1310–1314.

(27) Huang, L.; Mühlenbernd, H.; Li, X.; Song, X.; Bai, B.; Wang, Y.; Zentgraf, T. Broadband Hybrid Holographic Multiplexing with Geometric Metasurfaces. *Adv. Mater.* **2015**.

(28) Tang, D.; Wang, C.; Zhao, Z.; Wang, Y.; Pu, M.; Li, X.; Gao, P.; Luo, X. Ultrabroadband Superoscillatory Lens Composed by Plasmonic Metasurfaces for Subdiffraction Light Focusing. *Laser Photonics Rev.* **2015**, *9*, 713–719.

(29) Luo, J.; Zeng, B.; Wang, C.; Gao, P.; Liu, K.; Pu, M.; Jin, J.; Zhao, Z.; Li, X.; Yu, H.; Luo, X. Fabrication of Anisotropically Arrayed Nano-Slots Metasurfaces Using Reflective Plasmonic Lithography. *Nanoscale* **2015**, *7*, 18805–18812.

(30) Pu, M.; Li, X.; Ma, X.; Wang, Y.; Zhao, Z.; Wang, C.; Hu, C.; Gao, P.; Huang, C.; Ren, H.; Li, X.; Qin, F.; Yang, J.; Gu, M.; Hong, M. H.; Luo, X. Catenary Optics for Achromatic Generation of Perfect Optical Angular Momentum. *Sci. Adv.* **2015**, *1*, e1500396.

(31) Li, Z.; Palacios, E.; Butun, S.; Aydin, K. Visible-Frequency Metasurfaces for Broadband Anomalous Reflection and High-Efficiency Spectrum Splitting. *Nano Lett.* **2015**, *15*, 1615–1621.

(32) Li, X.; Pu, M.; Zhao, Z.; Ma, X.; Jin, J.; Wang, Y.; Gao, P.; Luo, X. Catenary Nanostructures as Highly Efficient and Compact Bessel Beam Generators. *Sci. Rep.* **2016**, *6*, 20524.

(33) Hakobyan, D.; Magallanes, H.; Seniutinas, G.; Juodkazis, S.; Brasselet, E. Tailoring Orbital Angular Momentum of Light in the Visible Domain with Metallic Metasurfaces. *Adv. Opt. Mater.* **2015**.

(34) Ciattoni, A.; Crosignani, B.; Di Porto, P. Vectorial Free-Space Optical Propagation: A Simple Approach for Generating All-Order Nonparaxial Corrections. *Opt. Commun.* **2000**, *177*, 9–13.

(35) Liu, T.; Tan, J.; Liu, J.; Wang, H. Vectorial Design of Super-Oscillatory Lens. *Opt. Express* **2013**, *21*, 15090–15101.

(36) Biener, G.; Niv, A.; Kleiner, V.; Hasman, E. Formation of Helical Beams by Use of Pancharatnam-Berry Phase Optical Elements. *Opt. Lett.* **2002**, *27*, 1875–1877.

(37) Verslegers, L.; Catrysse, P. B.; Yu, Z.; White, J. S.; Barnard, E. S.; Brongersma, M. L.; Fan, S. Planar Lenses Based on Nanoscale Slit Arrays in a Metallic Film. *Nano Lett.* **2008**, *9*, 235–238.

(38) Zhan, Q. Properties of Circularly Polarized Vortex Beams. *Opt. Lett.* **2006**, *31*, 867–869.

(39) Yue, F.; Wen, D.; Xin, J.; Gerardot, B. D.; Li, J.; Chen, X. Vector Vortex Beam Generation with a Single Plasmonic Metasurface. *ACS Photonics* **2016,** DOI: 10.1021/acsphotonics.6b00392.

(40) Genevet, P.; Yu, N.; Aieta, F.; Lin, J.; Kats, M. A.; Blanchard, R.; Scully, M. O.; Gaburro, Z.; Capasso, F. Ultra-Thin Plasmonic Optical Vortex Plate Based on Phase Discontinuities. *Appl. Phys. Lett.* **2012**, *100*, 13101.

(41) Pu, M.; Zhao, Z.; Wang, Y.; Li, X.; Ma, X.; Hu, C.; Wang, C.; Huang, C.; Luo, X. Spatially and Spectrally Engineered Spin-Orbit Interaction for Achromatic Virtual Shaping. *Sci. Rep.* **2015**, *5*, 9822.

(42) Khorasaninejad, M.; Chen, W. T.; Devlin, R. C.; Oh, J.; Zhu, A. Y.; Capasso, F. Metalenses at Visible Wavelengths: Diffraction-Limited Focusing and Subwavelength Resolution Imaging. *Science* **2016**, *352*, 1190.

(43) Brasselet, E.; Gervinskas, G.; Seniutinas, G.; Juodkazis, S. Topological Shaping of Light by Closed-Path Nanoslits. *Phys. Rev. Lett.* **2013**, *111*, 193901.

(44) Bozinovic, N.; Yue, Y.; Ren, Y.; Tur, M.; Kristensen, P.; Huang, H.; Willner, A. E.; Ramachandran, S. Terabit-Scale Orbital Angular Momentum Mode Division Multiplexing in Fibers. *Science* **2013**, *340*, 1545–1548.

For Table of Contents Use Only

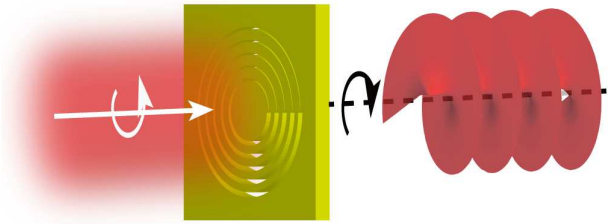

Title: Merging geometric phase and plasmon retardation phase in continuously shaped metasurfaces for arbitrary orbital angular momentum generation

Authors: Yinghui Guo, Mingbo Pu, Zeyu Zhao, Yanqin Wang, JinJin Jin, Ping Gao, Xiong Li, Xiaoliang Ma, and Xiangang Luo